JOURNAL OF MATERIALS SCIENCE 24 (1989) 3934–3946

Magnesium–lithium alloys in metal matrix composites – A preliminary report

J. F. MASON, C. M. WARWICK, P. J. SMITH, J. A. CHARLES, T. W. CLYNE
Cambridge University, Department of Materials Science and Metallurgy, Pembroke Street, Cambridge CB2 3QZ, UK

Procedures are described for the fabrication of fibrous composites based on magnesium–lithium alloys as a matrix. Such composites have been produced containing planar random and aligned (continuous and discontinuous) fibres of carbon, alumina and silicon carbide. For all of these, except silicon carbide whiskers, significant fibre degradation occurred, during fabrication or subsequent heat treatments, either by chemical reaction or by grain boundary penetration of lithium. Further consequences of the high atomic mobility exhibited by the matrix are manifest in the mechanical behaviour of the composites. Although considerable property enhancement is possible by fibre reinforcement, a significant diffusional contribution to the stress relaxation mechanisms results in a dependence of work hardening rate and failure strain on temperature and strain rate, even around room temperature and at relatively high strain rates. It is concluded that, although the system presents many practical difficulties, it is worthy of further study.

1. Introduction

A variety of light alloys have been extensively explored as matrices for metal-based composite materials. For example, magnesium has been reinforced with boron [1], silicon carbide [2], graphite [3] and alumina [4–6]. Among other publications are a number dealing with aluminium–lithium matrices [7], and at least one in which pure lithium is considered [8]: this latter study explored the chemical compatibility between molten lithium and various candidate reinforcements, reporting a variety of chemical attack phenomena. However, there appear to be no reports in the open literature on the use of magnesium–lithium alloys in metal matrix composites.

The Mg–Li phase diagram is shown in Fig. 1 [9]. No intermetallic compounds are formed and the lithium body-centred cubic structure exhibits solid solubility for magnesium up to about 70 at % (90 wt %). An alloy of Mg–11 wt % Li displays a combination of high melting point (about 593° C), low density (about 1.4 $Mg\,m^{-3}$) and very high ductility. Detailed work on the fabrication and properties of Mg–Li alloys was carried out by Jackson *et al.* in 1949 [10]. This study highlighted the difficulties of strengthening by conventional methods materials based on the bcc matrix. Attempts to develop precipitation-hardening systems were frustrated by overageing effects at room temperature. This is apparently a result of very high vacancy mobility, which also encourages dislocation climb and minimizes work hardening. The material exhibits pronounced creep at room temperature.

It might be expected from the above that Mg–Li alloys would be attractive candidates for reinforcement with ceramic fibres or particles. In practice they present certain difficulties, not least in terms of fabrication route development and other problems related to their high chemical reactivity. In the present paper an introduction is given to some of the main features observed when preparing, examining and testing Mg–Li composites of various types. The very high diffusional mobility that the alloys exhibit (for example, the diffusivity of lithium at 420° C in Mg–10 wt % Li is reported [11] as $10^{-10}\,m^2\,sec^{-1}$) gives rise to a variety of interesting effects, some of which may be instructive in exploring fundamental aspects of the behaviour of metal matrix composites. It is intended in further publications to explore certain features of these composites in greater depth.

2. Experimental procedure

2.1. Alloy preparation

A number of alloys have been prepared, including both single phase (bcc) and two phase binary Mg–Li alloys and multicomponent alloys. In particular, a Mg–10.3Li–6Al–6Ag–4Cd alloy was prepared, this being one of the more effective precipitation-hardening compositions reported in the original survey [10]. In general, however, much of the work in the current programme has involved single phase binary material with a composition just above the congruent melting point (10.5 wt %), typically about 12 wt %. Alloys near the congruent point might be expected to exhibit fewer segregation problems during solidification than other compositions, but in practice a pronounced tendency towards macrosegregation during processing is characteristic of the Mg–Li alloy system as a whole.

The alloys were prepared by heating solid pieces of magnesium and lithium in a tall, covered steel tube, being continuously flushed with argon, in a gas furnace. The melt was brought to a suitable superheat

0022–2461/89 $03.00 + .12

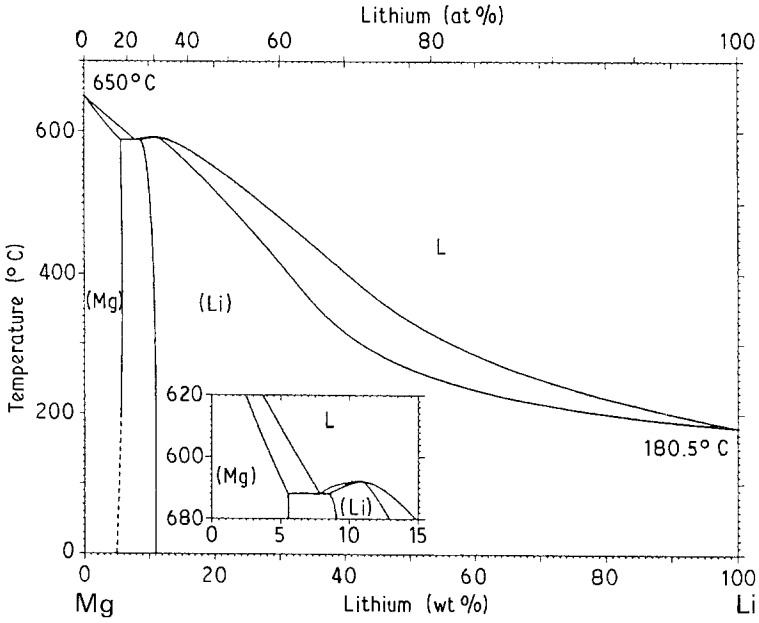

Figure 1 The Mg–Li phase diagram [9].

and then strongly agitated with a stirrer for about 5 to 10 minutes. The melt was then allowed to solidify *in situ*, with the cooling enhanced by air jets directed onto the tube. Cylindrical ingots of about 1 kg mass were produced in this way, the steel tube being removed by machining. Providing that solidification took place fairly rapidly, this process yielded ingots of good chemical homogeneity, although it was sometimes necessary to discard portions from the top and bottom because of a degree of gravity segregation. There is little tendency towards loss of composition control via volatilization, as the two elements exhibit rather similar vapour pressures over the temperature range of interest.

2.2. Composite fabrication

All of the composites described here were manufactured by squeeze infiltration. In Fig. 2 a schematic illustration shows the design of the equipment used. The melt is allowed to fall onto a preform (an assembly of ceramic fibres) by the withdrawal of a sliding crucible base. Pressure is then applied to the melt via a hydraulic ram which passes through the crucible. Typically, pressures of around 30 MPa were applied, and maintained during the period of melt solidification. This is in all cases more than sufficient to ensure that the melt penetrates the fibre array (see below), but the excess pressure can be beneficial in facilitating the liquid feeding through the mushy zone required to accommodate the freezing contraction and avoid porosity. The entire operation is carried out in a vacuum chamber under controlled atmosphere.

A range of reinforcements has been employed. These are listed in Table I, which shows calculated values for the pressures needed to infiltrate and to damage the fibre array, and the minimum melt super-

TABLE I Calculated critical parameters for infiltration of various preforms

Preform Structure			Infiltration Parameters		
Fibre	Assembly Geometry	V_f (%)	Infiltration pressure* (MPa)	Damage onset pressure (MPa)	Minimum superheat† (K)
"Saffil" Al_2O_3	Planar random (with crosslinks)	10	0.21	0.33	50
		25	0.41	1.29	150
		40	0.60	2.60	300
"Nicalon" SiC (PCS multifilament)	Unidirectional (axial) bundle	30	0.05	–	115
		60	0.10	–	500
		80	0.14	–	1050
"Sigma" SiC (CVD monofilament)	Planar random (no crosslinks)	10	0.007	~0.8	35
		25	0.015	~3.4	110
		40	0.022	~7.0	220
Carbon	Planar random (with crosslinks)	10	0.08	0.34	40
		25	0.15	1.35	115
		40	0.23	2.70	230
"Tokawhisker" SiC	Planar random (with crosslinks)	10	1.3	1.3	35
		25	2.4	5.2	110
		40	3.6	10.4	220

*Using a value or the melt surface tension of $0.55\,J\,m^{-2}$

†Assuming a preform temperature of 350° C and a specific heat of $1.8\,MJ\,m^{-3}\,K^{-1}$ for the melt.

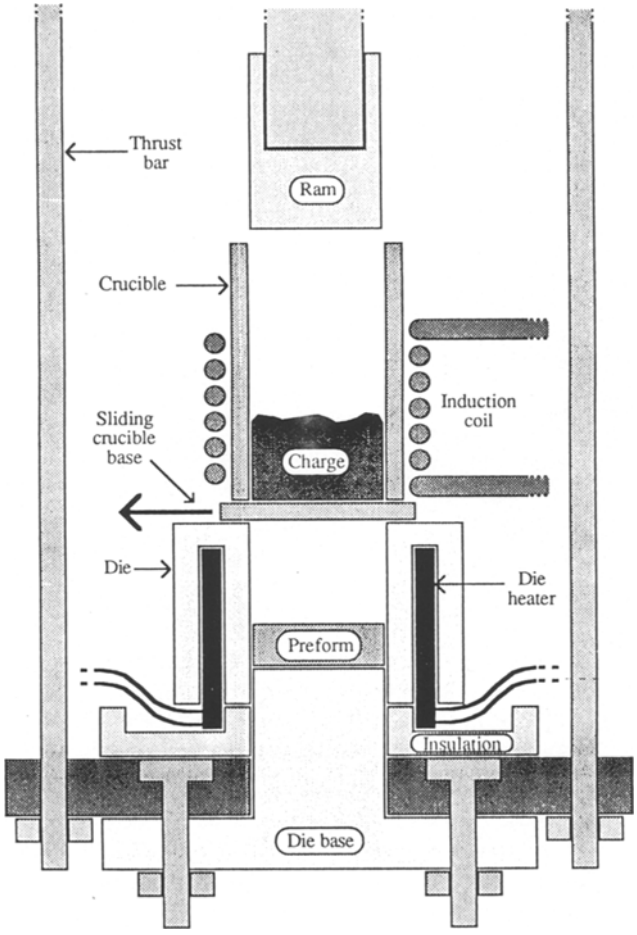

Figure 2 Schematic illustration of the squeeze infiltration operation.

heat to avoid premature solidification. The basis of these calculations is described in a previous publication [13]. These calculations suggest that infiltration should precede (and thus preclude) fibre damage for all of the composites produced in the present work, which is consistent with the observed absence of fractured fibres in the microstructures. The melt superheats employed were above the calculated minimum values for all of the planar random preforms (which contained up to about 25 vol % fibre): in general, problems associated with premature solidification were minimal in these cases. The "Nicalon" bundle, on the other hand, which was packed in a copper tube, contained over 60 vol % fibre: the requisite superheat of over 500 K is very difficult to achieve because of high volatilization losses. It was indeed found that incomplete infiltration as a result of premature solidification was common with this system. However, it was found that complete infiltration was possible using a thin-walled tube, provided that the melt was allowed to surround the tube before the pressure was applied. This presumably preheated the fibre array sufficiently to avoid the problem. (As the system is enclosed in a vacuum chamber, it is otherwise difficult to preheat the preform to a temperature greater than that of the die.)

In the case of the silicon carbide whisker-reinforced material, attempts were made to produce unidirectionally aligned material from the as-cast planar random composites by extrusion processing. Following experimental investigations of the role of extrusion conditions in controlling the degree of fibre damage in aluminium-based composites [14], a combination of low die angle, high extrusion temperature and modest extrusion ratio was used to produce good alignment of whiskers with relatively high aspect ratios. In practice, certain developments of the preform production procedure have been necessary in order to generate material of high microstructural quality. For example, the nature, concentration and distribution of the preform binding agent is important, particularly in view of the tendency of this melt to react with most binders during infiltration. In addition, inhomogeneities of fibre distribution can become enhanced during extrusion as a result of the concentration of plastic strain in the highly ductile, fibre-depleted regions, leading to microstructures of the type shown in Fig. 3a. This can, however, be overcome by improved process control leading to uniform, homogeneous structures, with preferential whisker alignment along the extrusion axis, of the type illustrated by Fig. 3b.

2.3. Microstructural examinations

Specimens were examined by optical, SEM, and TEM techniques, before and after various thermal and mechanical treatments. Most of the problems of specimen preparation are those that arise from the chemical reactivity of the system. Exposed surfaces corrode quite rapidly, particulary in the presence of moisture. In particular, lithium loss from the matrix can be significant at room temperature. (For example, an initially single phase matrix can, when examined by X-ray diffraction – sampling the superficial 50 μm or

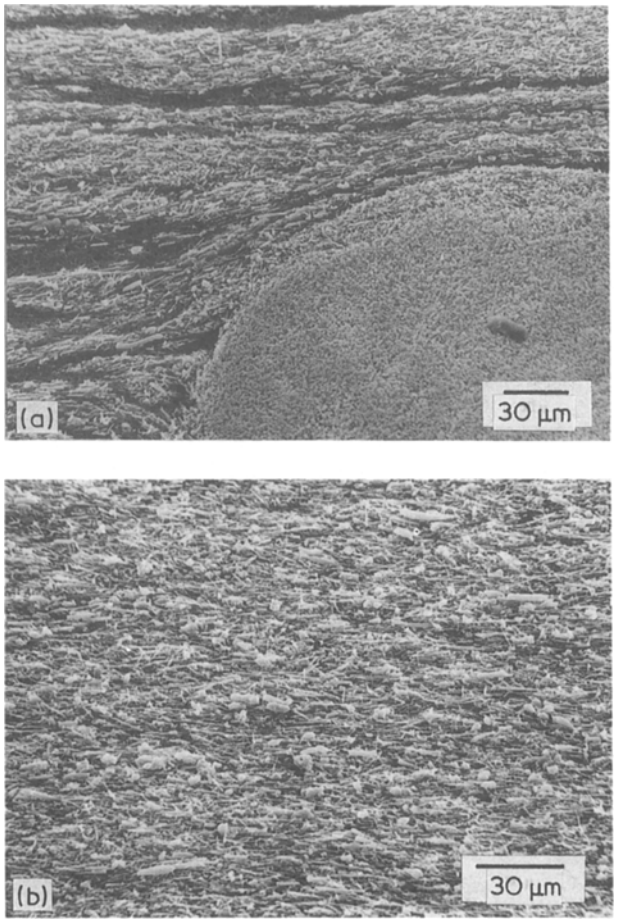

Figure 3 SEM micrographs of deep-etched Mg–12 wt % Li/20 vol % SiC "Tokawhisker", parallel to the extrusion direction (a) showing a dense whisker "ball" resulting from inadequate whisker dispersion in the original preform and (b) exhibiting a homogeneous and well aligned whisker distribution.

so – given rise to detectable h c p phase peaks on exposure to air for a few days.) Preparation of TEM specimens is particularly hampered by such lithium loss: conventional ion beam thinning results in complete conversion of the thinned region of the matrix to the h c p phase. This effect can be reduced by carrying out the ion beam milling at low temperature, but the foil is then prone to oxidation during transfer to the microscope. Nevertheless, useful examination of any changes induced in the ceramic reinforcement is possible by TEM techniques. Deep etching to reveal fibre distributions by SEM examination was carried out by using 1% sulphuric acid as the etchant.

2.4. Mechanical testing

A variety of tests have been carried out, including tensile testing with both clip gauges and adhesive strain gauges. In addition, both macrohardness and *in situ* matrix microhardness have been measured in various composites. A short comparative series of impact fracture energy tests was also carried out (using non-standard specimen dimensions, but with a geometry very similar to that of the standard Izod test). The specimens were unnotched and were oriented so that the fibre plane was parallel to the plane of pendulum motion.

3. Microstructural stability

In a matrix of such high chemical activity, one of the prime concerns is with matrix–fibre reaction, and its affect on mechanical behaviour. There may be scope for such reaction to occur either during processing or in service. Of the candidate reinforcements that are freely available, carbon, alumina and silicon carbide have been employed in the present study.

3.1. Carbon multifilament (in planar random felt)

Little attention was devoted to carbon, as it soon became clear that extensive carbide formation takes place very rapidly on exposure to a Mg–Li melt. Fig. 4 shows the microstructure in the as-fabricated form. The fibres, have been extensively attacked, and lithium-depleted (h c p phase) regions of matrix created around them. X-ray diffraction data indicated that Li_2C_2 had been formed. A degree of fibre cracking was also observed.

3.2. Alumina staple fibre ("Saffil")

This fibre contains about 5 wt % SiO_2 and is primarily in the form of the δ-Al_2O_3 phase [15, 16]. In the as-fabricated form there was little obvious evidence of gross chemical attack; a typical microstructure is shown in Fig. 5. There was, however, considerable evidence that the (silica-based) binder was being rapidly dissolved on contact with the melt and then carried through the preform, becoming concentrated

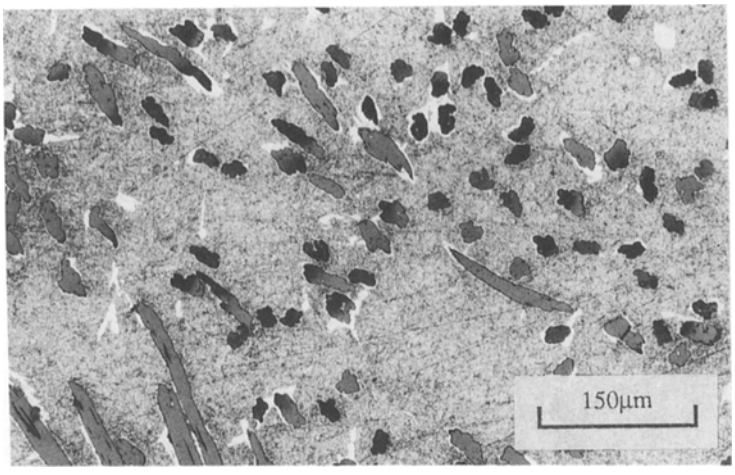

Figure 4 Optical micrograph of as-fabricated Mg–12 wt % Li/15 vol % C planar random composite.

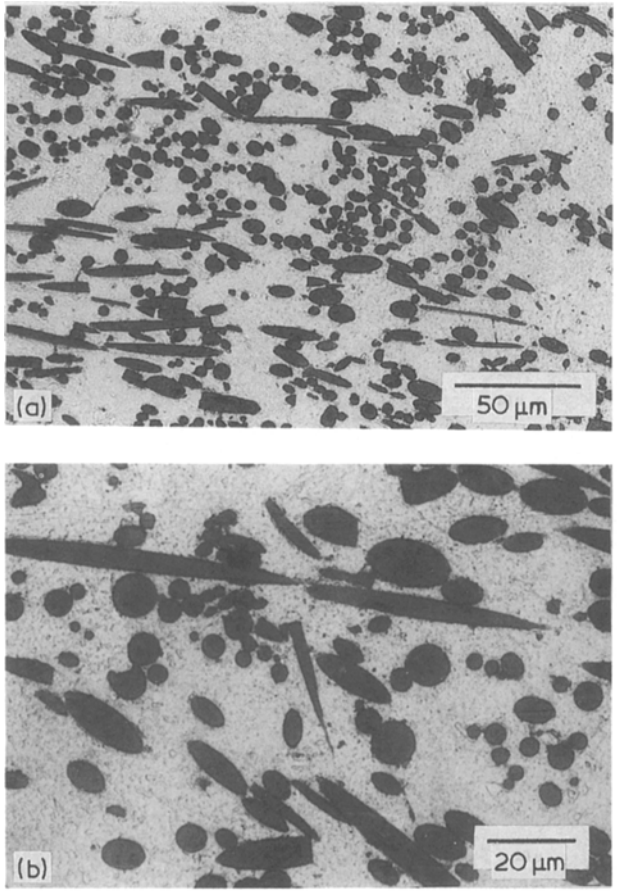

Figure 5 Optical micrographs of a longitudinal section of a Mg–12 wt % Li/24 vol % "Saffil" composite.

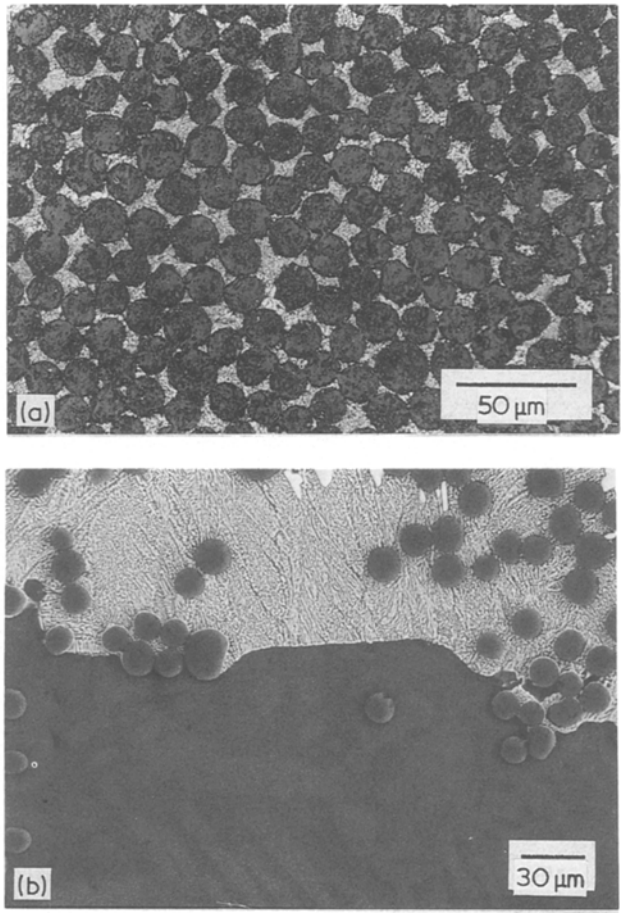

Figure 6 Transverse sections of uniaxial Mg–12 wt % Li/60 vol % "Nicalon" composite: (a) Optical micrograph of high fibre content area and (b) backscattered SEM micrograph of a region of variable fibre population.

in the lower regions. In these areas, certain precipitates, notably Mg_2Si, often appeared in some profusion. In addition to the binder reaction effects, there were indications that a degree of interaction was taking place with the matrix. The silica in "Saffil" is concentrated on the free surface and at grain boundaries [16]. Reduction of the surface layer was probably responsible in part for the observed high fibre–matrix bond strength, but penetration of lithium down the grain boundaries also appeared to take place, leading to severe embrittlement of the fibres (see Section 4.1 and Fig. 14).

3.3. Silicon carbide fibres

3.3.1. "Nicalon" multifilament

This fibre, which is produced by pyrolysis of polycarbosilane [17], is not pure SiC; the product used here has a very fine grain size (about 2 nm), with about 15 wt % free carbon and 25 wt % free silica present in amorphous form at the grain boundaries [18]. Composites produced by axial infiltration of fibre bundles exhibited good matrix penetration, even into regions of very high fibre volume fraction, an example of which is shown in Fig. 6a. However, it became clear that this system was highly unstable microstructurally. In particular, the fibres tend to absorb lithium very rapidly. In Fig. 6b, which is a backscattered SEM image, the lithium-depleted regions appear light. It can be seen that these occur around the fibres: in areas of high fibre population the depletion has been sufficient to cause formation of the hcp–bcc eutectic structure.

This lithium penetration, which occurs during and immediately after infiltration, is sufficient to cause differential effects along the infiltration axis. Furthermore, although the change in matrix composition is exaggerated by the high volume fraction of fibre in the uniaxial bundles, the consequences for the fibre itself are greater at lower fibre loadings. For example, Fig. 7, which shows structures at different heights in a planar random Nicalon preform, illustrates that the fibre degradation is pronounced. (This is less obvious near the base, where the melt contact time and high temperature exposure period are shorter.) Experiments in which the Nicalon fibre was exposed to lithium vapour [19] confirmed that the element is rapidly absorbed up to very high levels ($\geqslant 30$ wt %), causing dramatic embrittlement.

3.3.2. "Sigma" CVD monofilament (tungsten core)

In the case of the large diameter CVD monofilaments, which are essentially pure SiC, there was no obvious evidence of progressive chemical reaction taking place – for example new X-ray peaks did not appear. Nevertheless, the fibres did tend to suffer pronounced degradation – apparently in the form of grain boundary attack. For example, it is clear from Fig. 8 that fibre cracking is widespread in the as-fabricated

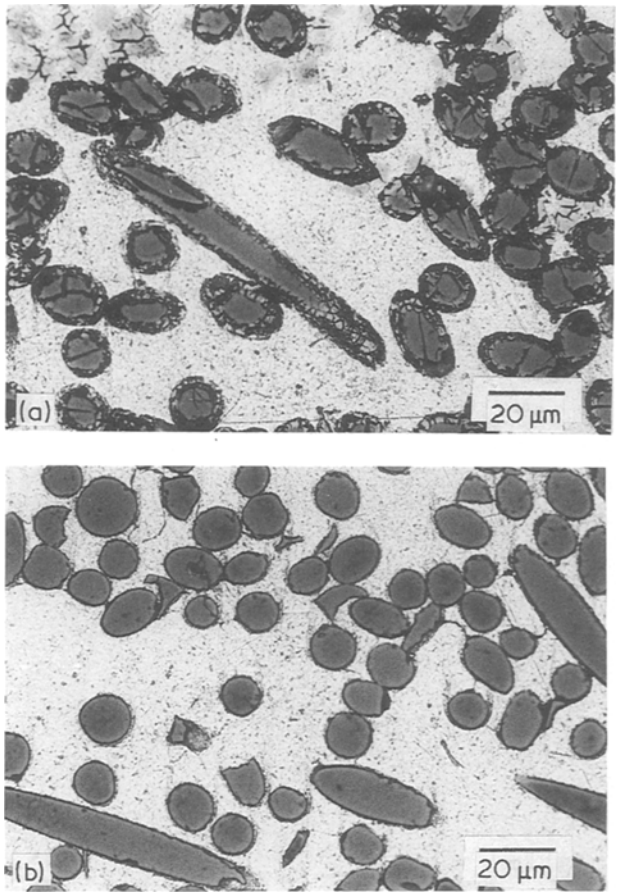

Figure 7 Optical micrographs of Mg–12 wt % Li/20 vol % "Nicalon" planar random composite parallel to the infiltration axis (a) about 3 mm above the base and (b) about 0.5 mm above the base.

condition, and becomes systematic and universal after heat treatment. The grain structure in these fibres is radial columnar [20] and there are strong indications that the observed cracking is of an intergranular type, generated by lithium penetration of the grain boundaries. Local lithium detection is, of course, far from easy to carry out quantitatively with any degree of confidence, but in the present case there is strong evidence for this mechanism. For example, in Fig. 9 a comparison is presented between the fracture surfaces of individual monofilaments broken manually before and after exposure of the fibres to lithium vapour. In the latter case (when the fibre is significantly embrittled) there is a clear tendency for cracks to follow intergranular paths across the section and along the fibre length (trends also observed in the composite). The progressive nature of the lithium penetration and accompanying crack formation on extending the heat treatment is illustrated by the histogram shown in Fig. 10. Finally it may be noted that monofilaments of this type can be protected against attack. For example, sputterdeposited diffusion barrier layers [21, 22] can be employed to isolate fibre and matrix. That these can be effective in the present case is illustrated in Fig. 11, which demonstrates that a Y_2O_3 layer of about 1 μm thickness can provide good protection against the ingress of lithium. (A device for continuous deposition of such layers onto long lengths of fibre, which is currently under development, should facilitate the production of composites incorporating such protection.)

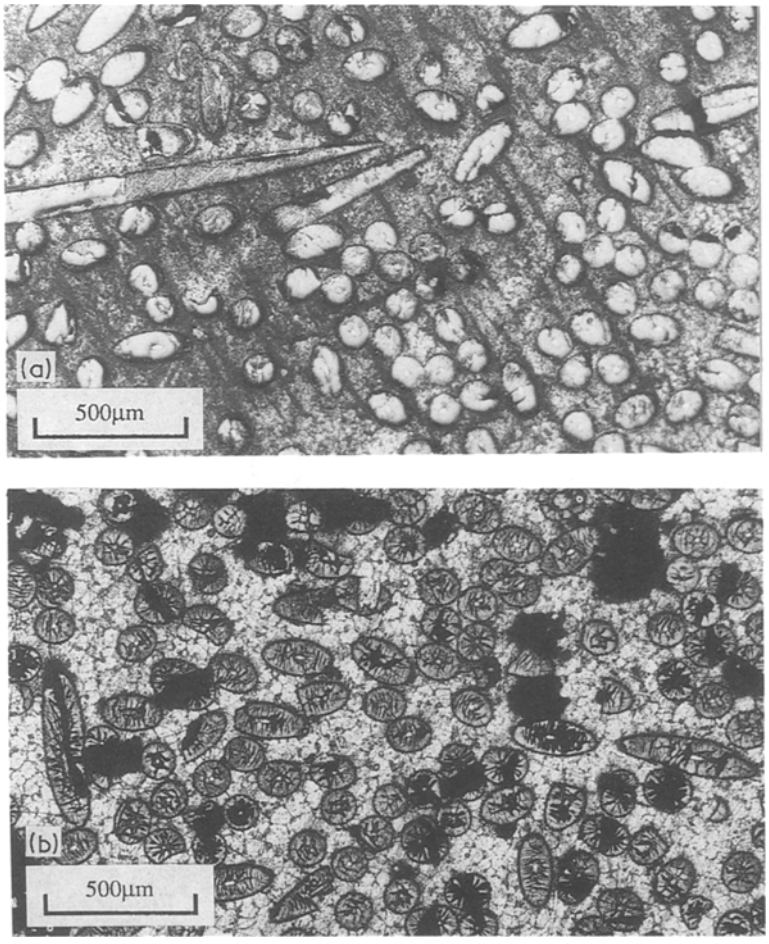

Figure 8 Optical micrographs of Mg–12 wt % Li/20 vol % "Sigma" planar random composite (longitudinal section) (a) as-fabricated and (b) after a heat treatment of 7 h at 400° C.

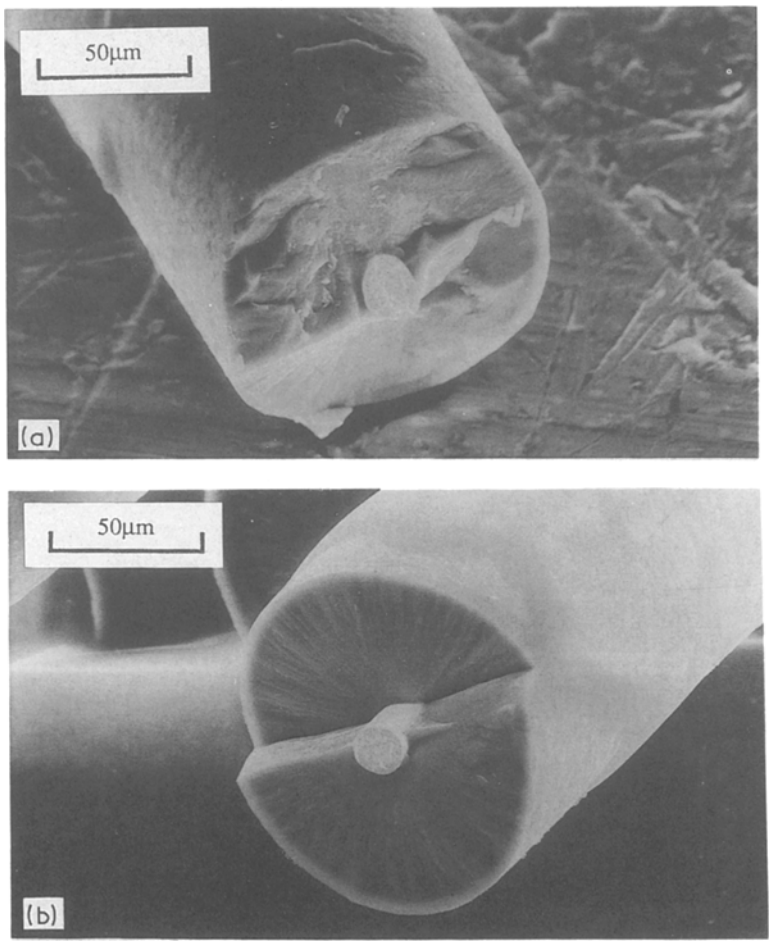

Figure 9 SEM micrographs of the fracture surfaces of individual "Sigma" fibres broken by hand (a) in the as-received condition and (b) after impregnation with lithium by exposure to lithium vapour (about 1 mbar for 18 h at 700° C).

3.3.3. "Tokawhisker" whiskers

It was found that the (single crystal) whiskers did not appear to suffer any chemical reaction on contact with the Mg–Li matrix, even after prolonged exposure to high temperature. For example, the TEM micrograph shown in Fig. 12b is of a specimen heated for about 12 h at 500° C. Although the matrix is fully hcp, having suffered extensive lithium loss during foil preparation, it is clear from Fig. 12 that the whisker surface has not been noticeably affected by this very severe heat treatment.

This observation should be considered in the light of thermodynamic information about the system. Among possible chemical reactions, the two listed below would appear the most likely

$$2Mg + SiC \rightarrow Mg_2Si + C \quad (1)$$

$$\Delta G^0_{600K} = -7(\pm 15)\,kJ\,mol^{-1}$$

$$2Mg + Li + SiC \rightarrow Mg_2Si + \tfrac{1}{2}Li_2C_2 \quad (2)$$

$$\Delta G^0_{600K} = -18(\pm 25)\,kJ\,mol^{-1}$$

In the absence of accurate information on the variations of activity with composition in the Mg–Li system, it is difficult to calculate the exact free energy changes for these reactions in the alloy. In any event, it should be noted that the probable errors in the experimental data [23–25] used in estimating the ΔG^0

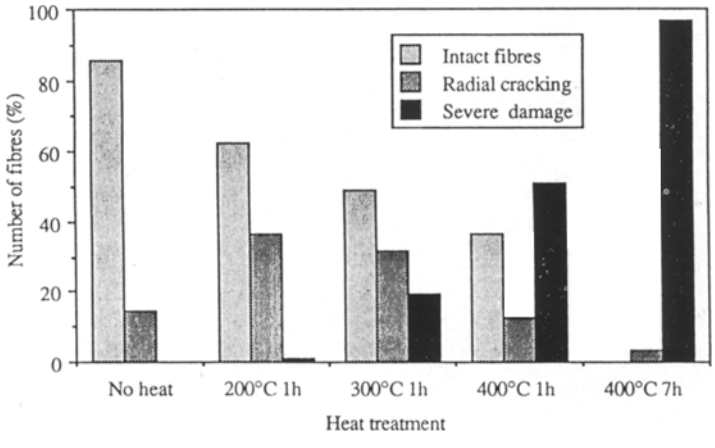

Figure 10 Histogram illustrating qualitatively the degree of fibre damage observed in Mg–12 wt % Li/20 vol % "Sigma" composites, as a function of heat treatment.

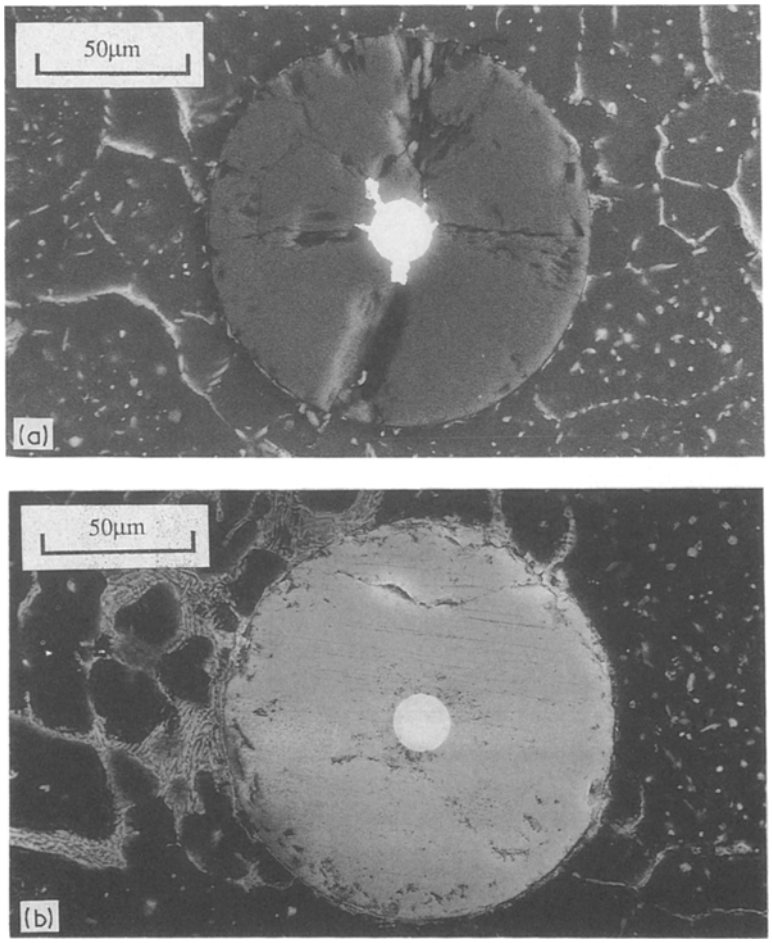

Figure 11 SEM images of single "Sigma" fibres embedded in a Mg–12 wt % Li matrix, after heat treatment for 1 h at 300° C, with the fibre (a) in the as-received condition (secondary electron) and (b) pre-treated by sputter-deposition of a layer of yttria (back-scattered electron).

values mean that both free energy changes may be of the opposite sign. This would be consistent with the current observations, in which the apparent absence of even a very thin reaction layer suggests that it is the lack of a thermodynamic driving force, rather than slow reaction kinetics, which is responsible for the stability of the system.

However, the difficulty of avoiding chemical reaction with the binder still remains. It was found that, in the presence of the whisker agglomerates shown in Fig. 3(a), there was a tendency for binder reaction products to be precipitated around the surface of these "balls". With the more uniform material subsequently produced, precipitation was more homogeneously distributed on a macroscopic scale, but still occurred preferentially on certain sites. With the whisker product used in the present work, this precipitation largely took the form of Mg_2Si sheaths formed around small (about 1 μm diameter) central cores of small, spherical transition metal silicides, such as CoSi and FeSi (present as impurities in the whiskers and originating from the manufacturing process). The resulting spherical precipitates, typically about 5 to 10 μm in diameter, are apparent in Fig. 13. There was, in addition, evidence of a limited amount of very fine scale precipitation on the surface of some of the whiskers [26].

4. Mechanical performance

4.1. "Saffil"-reinforced composites

A summary of the mechanical property data obtained with the planar random "Saffil" reinforcement is shown in Table II. The Mg–12 wt %Li composites were tested in the as-cast condition, while the age-hardening matrix material was first solution treated and aged using recommended procedures [10]. Only two tensile tests were carried out for each case, while the hardness and impact energy data all represent the mean of at least three measurements.

Comparison between the two matrices in the unreinforced form reveals relatively little strengthening (although the hardness is raised) and considerable embrittlement resulting from the precipitation. This reflects the presence of a considerable quantity of second phase, in a rather coarse dispersion. Reinforcement of the precipitation-hardened matrix led to appreciable strengthening, but this was limited by the brittleness of the matrix, which is clearly unsuited to fibre reinforcement. The single phase matrix, on the other hand, gave more encouraging results, although one of the tensile specimens with 24 vol % reinforcement clearly failed prematurely (at the shoulder). In fact, microstructural examination of strained material revealed that the fibres themselves were weaker than expected. For example, in the structures shown in Figs 14a and 14b, the fibres are exhibiting extensive internal cracking. This may be contrasted with the appearance in Fig. 14c of the same fibres in an Al–Mg matrix subjected to a similar tensile strain. Although cracks are also appearing in these fibres, appreciable lengths between these cracks (along which the fibre stress builds up) appear to be sound. This embrittlement with the Mg-Li matrix, which is apparently due to grain boundary penetration of lithium (the grain

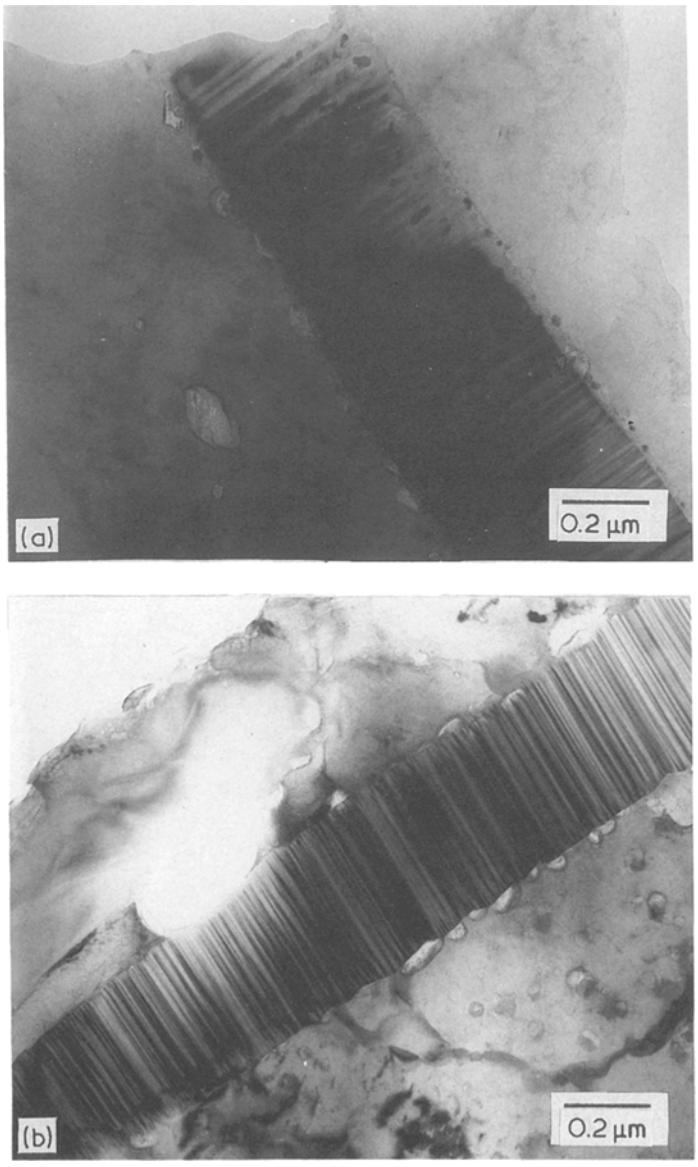

Figure 12 TEM bright field micrographs of whiskers in a Mg–12 wt % Li/20 vol % "Tokawhisker" planar random composite (a) as-fabricated and (b) after heat treatment for 280 h at 500° C.

size is about 50 nm [16]), presumably limits load transfer to the fibre. The significant enhancement of work-hardening rate and hence tensile strength, which is nevertheless observed, may be attributed largely to the build-up of back-stresses in the matrix as it deforms, imposed by the constraint that its local shape change must be compatible with that of the ceramic (which will be small and elastic). This effect is illustrated by the fact that, with increasing fibre loading, not only the macrohardness, but also the microhardness of the matrix, rises significantly.

4.2. "Tokawhisker"-reinforced composites

Tensile test data are presented from "Tokawhisker"-

TABLE II Summary of mechanical property data for "Saffil" reinforced planar random composites

Matrix	"Saffil"	Tensile testing		Mean Vickers hardness		Mean impact fracture energy	
	Volume fraction (%)	UTS (MPa)	Failure strain (%)	Macro ($kg\,mm^{-2}$)	Micro (matrix) ($kg\,mm^{-2}$)	$s/t = 3.5$ ($kJ\,m^{-2}$)	$s/t = 7$ ($kJ\,m^{-2}$)
Mg-12Li	0	70	> 6	35	42	> 90	> 600
		80	> 8				
	12	200	3.5	96	77	30	37
		220	2.1				
	24	280	2.0	113	81	–	–
		105	0.6				
Mg-10.3Li-6Al-6Ag-4Cd	0	85	0.4	93	85	13	17
		95	0.4				
	12	170	0.3	103	85	4	3
		165	0.3				
	24	145	0.3	145	95	2	2
		140	0.5				

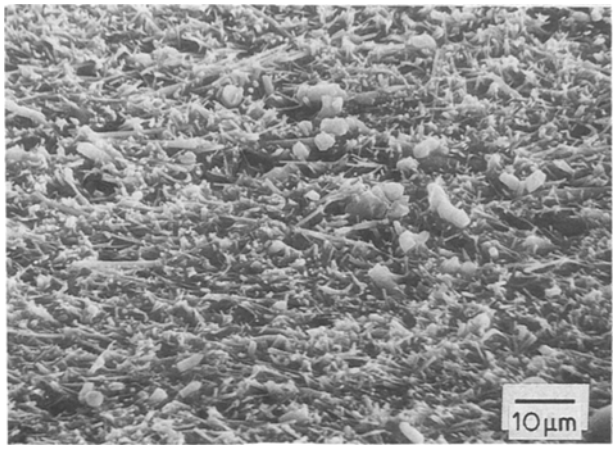

Figure 13 SEM micrograph of a deep-etched Mg–12 wt % Li/20 vol % "Tokawhisker" composite, showing the spherical inclusions referred to in the text.

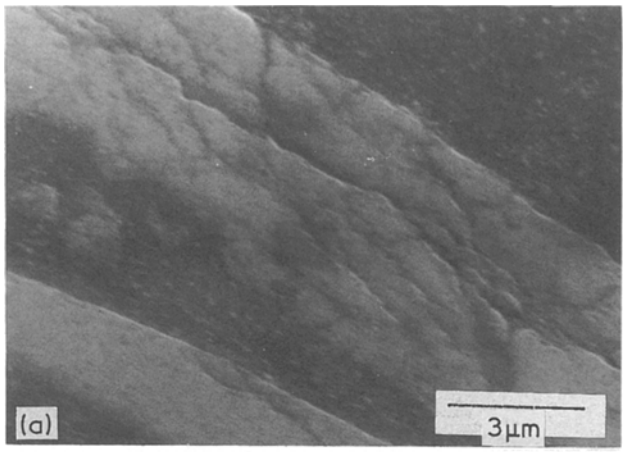

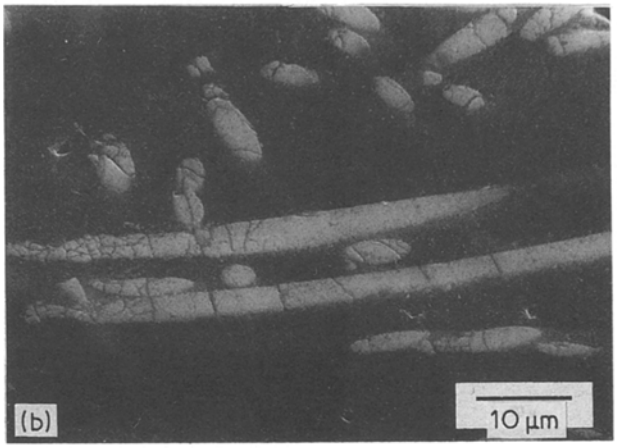

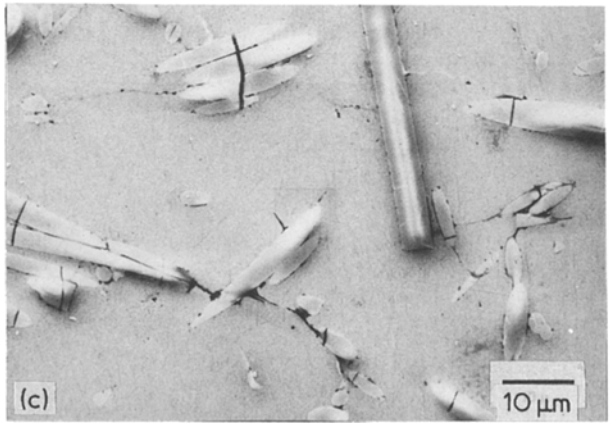

Figure 14 SEM micrographs of polished longitudinal sections of 12 vol % "Saffil" composites after tensile testing (to a few percent strain) (a) and (b) with a Mg–12 wt % Li matrix and (c) with an Al–25 wt % Mg matrix.

reinforced composites in which a homogeneous distribution of whiskers and of binder reaction products was achieved. The results are summarized in Table III and a typical set of three stress–strain curves is shown in Fig. 15. The improvements observed on generating whisker alignment by extrusion are expected, given that a relatively high mean aspect ratio was maintained. (With a matrix exhibiting such a low yield stress, simple shear lag theory predicts a large critical aspect ratio for this system, of about 100: given that the as-received whiskers typically have aspect ratios of about 100 to 500, this suggests, in a crude sense, that minimization of whisker fracture during processing will be of significant benefit.) Also of interest are the effects of strain rate and temperature. Clearly, high strain rate and low temperature increase the work-hardening rate and decrease the failure strain, suggesting a reduced scope for local stress relaxation in the matrix around the fibres. (Such a strong effect of strain rate at room temperature is unusual. For example, previous work [27, 28] on aluminium alloys reinforced with silicon carbide whiskers reported only very small effects on the stress–strain curve, even though a much larger range of strain rate was covered.) Comparison between the fracture surfaces for low and high strain rates, shown in Fig. 16, reveals a similar overall morphology, with local dimples around exposed whisker ends and limited pull-out in both cases. There are, however, suggestions of multiple cracking at the high strain rate, an effect also noted with the low test temperature. TEM studies have revealed [26] little evidence of fibre fracture or matrix cavitation, although the latter may take place more readily with low temperature and high strain rate.

5. Summary and conclusions

The Mg–Li system exhibits a number of interesting features, in addition to its attractive combination of relatively high modulus and very low density. Many of these features are associated with the very high atomic mobility of lithium, even at relatively low temperatures. Although data on this aspect are in short supply, it seems probable that, even in alloys containing up to 70 at %Mg (90 wt %), which exhibit high melting points (approaching 600° C), both the vacancy concentration and the lithium atom jump frequency are exceptionally high, even at room temperature. This results, not only in great mobility for both vacancies and lithium atoms, but also in rapid transport of other solute species. Among other effects, this leads to rapid coarsening of precipitates: in combination with rapid dislocation climb, this destroys the efficiency of conventional precipitation hardening mechanisms.

The mobility of the lithium atoms, together with their high chemical activity, also affects the viability of mechanically incorporated inclusions such as ceramic fibres. Although a satisfactory fabrication route has

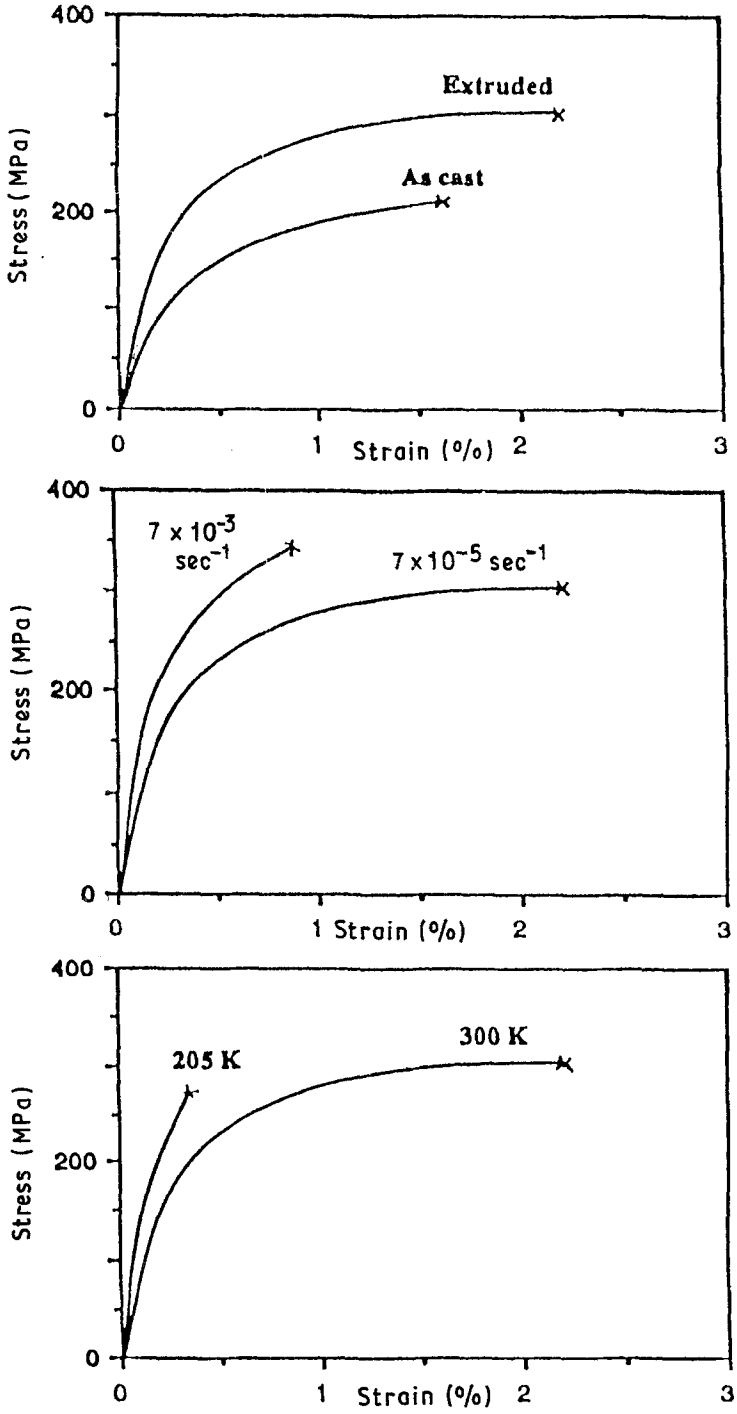

Figure 15 Three stress–strain curves for different Mg–12 wt % Li/20 vol % "Tokawhisker" composites and test conditions.

TABLE III Tensile testing data for Mg–12 wt % Li/20 vol % SiC "Tokawhisker"

Test specimen (3 of each)	*E* (GPa)		UTS (MPa)		Strain to failure (%)	
	Mean	S.D.	Mean	S.D.	Mean	S.D.
Unreinforced Alloy Test temperature 300 K Strain Rate 7 × 10^{-5} sec^{-1}	45	–	~75	–	> 10	–
Extruded material Test temperature 300 K Strain rate 7 × 10^{-5} sec^{-1}	96	14.0	302	2.0	2.3	0.33
Extruded material Test temperature 300 K Strain rate 7 × 10^{-2} sec^{-1}	112	15.6	338	6.5	0.84	0.05
Extruded material Test temperature ~200 K Strain rate 7 × 10^{-5} sec^{-1}	125	17.5	279	37.1	0.43	0.08
As-cast material Test temperature 300 K Strain rate 7 × 10^{-5} sec^{-1}	69	10.0	200	9.5	1.43	0.27

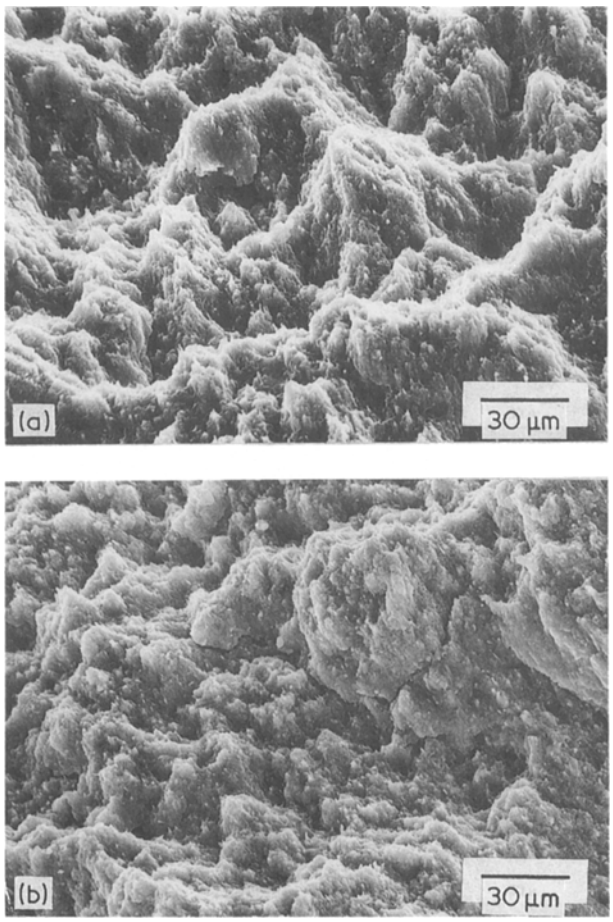

Figure 16 SEM micrographs of fracture surfaces from Mg–12 wt % Li/20 vol % "Tokawhisker" extruded composites tested at room temperature with strain rates of (a) $7 \times 10^{-5}\,sec^{-1}$ and (b) $7 \times 10^{-3}\,sec^{-1}$.

been developed for making composites based on the Mg–Li matrix, the choice of reinforcement is severely restricted by the reactivity aspects. Basically, of the reinforcements commonly available in fibrous form, only silicon carbide whiskers remain stable: the others all undergo highly deleterious chemical attack and /or grain boundary penetration. Although the magnesium is often as active in chemical terms as the lithium, it is, in many cases, the very fast kinetics associated with the latter that is responsible for an unacceptable degree of degradation occurring during fabrication.

Further consequences of high atomic mobility are manifest in the mechanical performance of the composites. Although a degree of strengthening is observed with alumina fibres which have been significantly embrittled by lithium penetration, the most promising data have been obtained with directionally aligned silicon carbide whiskers. Considerable enhancements of UTS and modulus have been obtained, although the latter are difficult to measure because of the very early onset of local plasticity. However, the behaviour under tensile loading has been shown to be strongly dependent on strain rate (between 10^{-2} and $10^{-4}\,sec^{-1}$) and temperature (between 200 and 300 K). This is associated with the kinetics of stress relaxation phenomena, particularly in terms of changes to the high local stress gradients around the fibre ends. It appears likely that there is a significant diffusive contribution to these relaxation mechanisms, even at the relatively high strain rates and low temperatures over which these experiments have been carried out. These aspects are currently the subject of further study.

Acknowledgements

The authors are grateful to BP plc for funding the project within which the work described here has been supported. Particular acknowledgement should be made to Dr C. W. Brown, Dr A. Begg and Mr J. Robertson, of the BP Research Centre, Sunbury-on-Thames, for active support and stimulating discussions.

References

1. T. W. CHOU, A. KELLY and A. OKURA, *Composites* **16** (1985) 187–206.
2. B. A. MICKUCKI, S. O. SHOOK, W. E. MERCER and W. G. GREEN, "Magnesium-matrix composites at DOW: Status Update", Conference International Magnesium Association, Los Angeles, (International Magnesium Association, 1986).
3. B. J. MacLEAN and M. S. MISRA, "Thermal mechanical behaviour of graphite/magnesium composites", 195-212, Proceedings Symposium. "Mechanical Behaviour of Metal-Matrix Composites" (1982), edited by J. E. Hack and M. F. Amateau, Metallurgical Society of AIME, Pennsylvania, (1983).
4. J. E. HACK, R. A. PAGE and G. R. LEVERANT, *Metall. Trans.* **15A** (1984) 1389–1396.
5. R. A. PAGE, J. E. HACK, R. SHERMAN and G. R. LEVERANT, *ibid.* **15A** (1984), 1397–1405.
6. J. T. EVANS, *Acta Metall.* **34** (1986) 2075–2083.
7. D. WEBSTER, *Metall. Trans.* **13A** (1982) 1511–1519.
8. R. T. SWANN and D. M. EASTERLING, *Composites* **15** (1984) 305–309.
9. A. A. NAYEB-HASHEMI, J. B. CLARK and A. D. PETTON, *Bull. Alloy Phase Diagrams* **5** (1984) 365–374.
10. J. H. JACKSON, P. D. FROST, A. C. LOONAM, L. W. EASTWOOD and C. H. LORIG, *Trans. TMS-AIME* **185** (1949) 149–168.
11. Y. IWADATE, M. LASSOUARI, F. LANTELME and M. CHEMLA, *J. Appl. Electrochem.* **17** (1987) 385–397.
12. F. D. RICHARDSON, "Physical chemistry of melts in metallurgy", (Academic, New York 1974).
13. T. W. CLYNE and J. F. MASON, *Metall. Trans.* **18A** (1987) 1519–1530.
14. C. A. STANFORD-BEALE and T. W. CLYNE, *Composites Sci. and Technol.* **35** (1989) 121–157.
15. J. D. BIRCHALL, *Trans. J. Brit. Ceram. Soc.* **82** (1983) 143–145.
16. G. R. CAPPLEMAN, J. F. WATTS and T. W. CLYNE, *J. Mater. Sci.* **20** (1985) 2159–2168.
17. S. YAJIMA, Y. HASEGAWA, J. HAYASHI and M. IIMURA, *ibid.* **13** (1978) 2569–2576.
18. G. SIMON and A. R. BUNSELL, *ibid.* **19** (1984) 3649–3657.
19. C. M. WARWICK and T. W. CLYNE, "Microstructural stability of fibrous composites based on Mg–Li alloys" in 3rd European Conference on Composite Materials, Bordeaux, edited by A. Bunsell, P. Lamicq and A. Massiah. (Elsevier, 1989) pp. 205–212.
20. R. WARREN and C. H. ANDERSSON, *Composites* **15** (1984) 16–24, 101–111.
21. R. C. MEHAN, M. R. JACKSON and M. D. McCONNELL, *J. Mater. Sci.* **18** (1983) 3195–3205.
22. R. R. KIESCHKE, R. E. SOMEKH and T. W. CLYNE, "The protection of SiC monofilaments against attack in metal matrix composites by sputter-deposited barrier layers", in preparation.
23. "Janaf Thermochemical Tables, 2nd edn", US Department of Commerce, NSRDS-NBS, 37 (1971).
24. I. BARIN and O. KNACKE, "Thermochemical Properties of Inorganic Substances", (Springer, New York, 1973).

25. A. YAMAMOTO/Tokai Carbon, UK patent GB211533A, (1983).
26. J. F. MASON and T. W. CLYNE, "Microstructural development and mechanical behaviour of whisker-reinforced Mg-Li alloys", in 3rd European Conference on Composite Materials, Bordeaux, edited by A. Bunsell, P. Lamicq and A. Massiah (Elsevier, 1989) pp. 213–220.
27. J. HARDING, M. TAYA, B. DERBY and S. PICKARD, "An investigation of the high strain rate deformation of SiC_w/2124 Al composite", Proc. ICCM VI/ECCM 2, 2.224-2.233, edited by F. L. Mathews, N. C. R. Buskell, J. M. Hodgkinson and J. Morton (Elsevier, London, 1987).
28. S. M. PICKARD, B. DERBY, J. HARDING and M. TAYA, *Scripta Metall.* **22** (1988) 601–606.

Received 29 September 1988
and accepted 23 January 1989